Catalytic Centers in the Thiamin Diphosphate Dependent Enzyme Pyruvate Decarboxylase at 2.4-Å Resolution†,‡

Fred Dyda,§,‖ William Furey,*,‖ Subramanyam Swaminathan,‖ Martin Sax,‖ Bruce Farrenkopf,§,⊥ and Frank Jordan⊥

Biocrystallography Laboratory, Veterans Administration Medical Center, P.O. Box 12055, University Drive C, Pittsburgh, Pennsylvania 15240, Department of Crystallography, 304 Thaw Hall, University of Pittsburgh, Pittsburgh, Pennsylvania 15260, and Department of Chemistry, Rutgers, The State University of New Jersey, 73 Warren Street, Newark, New Jersey 07102

Received February 3, 1993; Revised Manuscript Received March 23, 1993

ABSTRACT: The crystal structure of brewers' yeast pyruvate decarboxylase, a thiamin diphosphate dependent α-keto acid decarboxylase, has been determined to 2.4-Å resolution. The homotetrameric assembly contains two dimers, exhibiting strong intermonomer interactions within each dimer but more limited ones between dimers. Each monomeric subunit is partitioned into three structural domains, all folding according to a mixed α/β motif. Two of these domains are associated with cofactor binding, while the other is associated with substrate activation. The catalytic centers containing both thiamin diphosphate and Mg(II) are located deep in the intermonomer interface within each dimer. Amino acids important in cofactor binding and likely to participate in catalysis and substrate activation are identified.

Thiamin diphosphate (ThDP,[1] Figure 1) is an essential cofactor in a number of metabolically critical enzymatic processes, especially in carbohydrate metabolism. ThDP-dependent enzymes include the large class of α-keto acid decarboxylases, both nonoxidative and oxidative, as well as the ketolases, enzymes that perform the biological counterpart of benzoin condensations. Slow, nonenzymatic decarboxylation by thiamin and thiazolium models has received much attention (Breslow, 1958; Crosby et al., 1970; Kluger, 1987), but progress in understanding the details of enzymatic catalysis has been slower due to the lack of crystal structures for representatives of these decarboxylases. Decarboxylation is thought to be initiated by formation of the C2 carbanion of ThDP, that forms a nucleophilic adduct with C2 of the substrate α-keto acid (Breslow, 1958), followed by decarboxylation of the adduct to a C2-α-carbanion/enamine whose fate then diverges depending on the task of the particular enzyme. Although thiazolium ions *per se* can perform many of the reactions, it was proposed that the 4′-amino group also participates in catalysis (Schellenberger, 1967). This would demand a conformation about the C5′-methylene bridge in ThDP that is virtually never found in crystal structures of thiamin compounds but is not excluded on the basis of the conformational flexibility predicted by both computational (Jordan, 1974, 1976) and NMR studies (Gallo & Sable, 1982). In addition to shifting the conformational equilibrium of, and activating, ThDP toward catalysis, the protein may also be providing a diminished dielectric constant (Crosby et al., 1970) and optimal orientation of substrate.

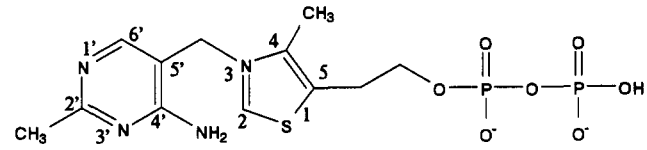

FIGURE 1: Schematic drawing of thiamin diphosphate indicating the atom numbering and labeling.

Pyruvate decarboxylase (PDC, EC 4.1.1.1), the simplest nonoxidative ThDP-dependent decarboxylase, catalyzes the reaction $CH_3COCOO^- + H_2O \rightarrow CH_3CHO + OH^- + CO_2$ and serves as a model for many related enzymes. Brewers' yeast PDC has a M_r of 250 000 and requires both ThDP and Mg(II) as tightly bound cofactors. It is subject to substrate activation (Boiteux, 1970) but can also be activated by the nondecarboxylatable substrate surrogate pyruvamide (Schellenberger et al., 1988). An X-ray structure determination of PDC was undertaken to address questions concerning the cofactor conformation, role of the protein in catalysis, and mechanism of activation. Due to the paucity of 3D structures on coenzyme-dependent decarboxylases of any sort, the results are of general significance as well. The PDC structure was initially reported at the American Crystallographic Association Summer Meeting (Dyda et al., 1992) and is now described in detail.

EXPERIMENTAL PROCEDURES

The structure of homotetrameric α_4 PDC (Farrenkopf & Jordan, 1992) from *Saccharomyces uvarum* was determined by the multiple isomorphous replacement method, supplemented with anomalous scattering, solvent flattening, and noncrystallographic symmetry averaging. The holoenzyme was initially crystallized (Dyda et al., 1990) by the sitting drop vapor diffusion method using PEG 8000 as the precipitating agent. However, these triclinic crystals were not directly suitable for structure determination due to long-term instability; thus a phase transformation to a more stable monoclinic form (space group $C2$, a = 142.0 Å, b = 74.7 Å, c = 120.0 Å, and β = 116.4°) was induced (Dyda et al., 1991) prior to data collection. In the monoclinic form the unit cell contains two tetramers but only one dimer (1126 amino acids)

† Supported in part by NIH Grant GM48195-01 (W.F.), NSF Grant DMB87-09758, the Rutgers University Busch Biomedical Fund, and Hoffmann-La Roche Inc., Nutley, NJ (F.J.).

‡ The crystallographic coordinates have been deposited with the Protein Data Bank, Chemistry Department, Brookhaven National Laboratory, Upton, NY 11973, under the file name 1PYD.

* Author to whom correspondence should be addressed.

§ In partial fulfillment of the Doctor of Philosophy degree.

‖ Veterans Administration Medical Center and University of Pittsburgh.

⊥ Rutgers University.

[1] Abbreviations: ThDP, thiamin diphosphate (the vitamin B1 coenzyme); PDC, pyruvate decarboxylase (EC 4.1.1.1); rms, root mean square; MIR, multiple isomorphous replacement; FOM, figure of merit; R factor, $\Sigma|FP(obs) - FP(cal)|/\Sigma FP(obs)$.

0006-2960/93/0432-6165$04.00/0

Table I: Native Data Statistics[a]

	phasing	refinement
no. of crystals	7	4
no. of measurements ($I > 2\sigma(I)$)	308455	192609
no. of unique reflections	32339	40681
completeness (%)	96 (2.75 Å)	92 (2.4 Å)
internal agreement (R_{sym}) (%)	8.6	6.9

[a] $R_{sym} = \Sigma\Sigma_i|I_i - \langle I\rangle|/\Sigma\langle I\rangle$, where I_i is the scale factor corrected intensity measurement for a reflection and $\langle I\rangle$ is the mean intensity for this reflection.

in the asymmetric unit. Native and derivative data were collected with Cu Kα radiation on a Siemens X100 area detector mounted on a Rigaku RU200 rotating anode source equipped with double-focusing Frank's mirrors. Data were collected with the Harvard software system (Blum et al., 1987), processed by XENGEN (Howard et al., 1987), and internally scaled with FBSCALE (Weissman, 1982). Five isomorphous derivatives were used along with limited anomalous scattering data from one of them. Although all derivatives were mercury compounds with major heavy atom sites essentially in the same locations (later shown to be in the vicinity of Cys 152 and Cys 221), the combination of small differences in the occupancies, the presence of additional minor sites, inclusion of anomalous scattering data, and noncrystallographic symmetry averaging nevertheless proved sufficient for phasing. Initial MIR-anomalous phases were calculated at 3-Å resolution (FOM = 0.67) and were subsequently improved and extended to 2.75 Å by solvent flattening and noncrystallographic symmetry averaging. The envelope encompassing one dimer was readily obtained by map inspection, and the averaging process was then straightforward, as we previously had shown (Dyda et al., 1990, 1991) that the tetramer has approximate 222 symmetry and had identified the directions of the noncrystallographic symmetry axes in both the triclinic and monoclinic forms. After 28 averaging/phase combination iterations, the resulting electron density map at 2.75-Å resolution was of excellent quality in most places, enabling roughly 85% of the chain to be initially traced unambiguously. All heavy atom refinement, phasing, solvent flattening, and averaging calculations were performed with the PHASES package (Furey & Swaminathan, 1990). Statistics related to the data and phasing process are given in Tables I and II, respectively. The electron density map was then displayed and interpreted with the interactive graphics programs O (Jones et al., 1991) for the protein and FRODO (Jones, 1978) for the cofactor. Since the sequence for PDC from *S. uvarum* is not presently known, model building assumed the PDC1 sequence from *Saccharomyces cerevisiae* (Hohmann, 1990)

Table II: Heavy Atom Parameters and Phasing Statistics[a]

derivative	type	x	y	z	B	occ	d	P_p	R_{iso}	R_C	R_K	no. of refl
K_2HgI_4	ISO	0.087	−0.233	0.126	20.0	1.00	3.0	2.07	0.15	0.58	0.10	18 054
		0.031	0.245	−0.064	20.0	0.93						
		0.135	0.076	−0.099	20.0	0.29						
		0.269	−0.049	0.244	20.0	0.18						
K_2HgI_4	ANO	0.087	−0.234	0.125	20.0	1.00	3.5	1.42			0.11	11 260
		0.036	0.243	−0.063	20.0	0.97						
		0.138	0.075	−0.095	20.0	0.34						
		0.268	−0.054	0.241	20.0	0.18						
$HgCl_2$	ISO	0.084	−0.235	0.125	6.0	0.90	3.0	1.24	0.16	0.58	0.12	19 654
		0.035	0.242	−0.061	8.0	0.92						
		0.142	0.079	−0.091	20.0	0.73						
		0.211	−0.054	0.189	38.0	0.70						
		0.218	−0.015	0.175	38.0	0.63						
		0.050	−0.287	0.096	38.0	0.17						
dimercury acetate	ISO	0.088	−0.233	0.126	20.0	0.95	3.0	1.68	0.18	0.55	0.18	14 007
		0.060	−0.233	0.092	20.0	0.27						
		0.029	0.245	−0.066	20.0	1.00						
		0.019	0.237	−0.043	20.0	0.24						
		0.136	0.071	−0.098	20.0	0.24						
		0.152	0.037	−0.075	20.0	0.26						
		0.216	−0.004	0.168	20.0	0.42						
		0.209	−0.004	0.192	20.0	0.43						
		0.250	−0.106	0.218	20.0	0.37						
		0.240	−0.146	0.212	20.0	0.29						
bakers' dimercurial	ISO	0.089	−0.233	0.126	20.0	1.00	3.0	1.28	0.15	0.68	0.15	17 440
		0.028	0.244	−0.066	20.0	0.97						
		0.130	0.075	−0.102	20.0	0.19						
		0.161	0.077	−0.151	20.0	0.13						
		0.150	0.123	−0.118	20.0	0.14						
		0.232	0.010	0.236	20.0	0.17						
		0.245	−0.019	0.267	20.0	0.16						
		0.234	−0.039	0.211	20.0	0.23						
		0.574	0.281	0.080	20.0	0.16						
		0.557	0.274	0.091	20.0	0.18						
dimercury malonate	ISO	0.084	−0.233	0.125	20.0	1.09	3.0	2.04	0.19	0.54	0.13	19 591
		0.037	0.243	−0.061	20.0	1.12						
		0.050	−0.287	0.095	20.0	0.16						
		0.142	0.080	−0.091	20.0	0.91						
		0.157	0.042	−0.075	20.0	0.62						
		0.218	−0.014	0.175	20.0	0.69						
		0.211	−0.052	0.189	20.0	0.75						
		0.881	0.140	0.157	20.0	0.10						

[a] d = minimum d spacing, in Å. B = isotropic temperature parameter, in Å^2. $R_{iso} = \Sigma|FPH^2 - FP^2|/\Sigma(FPH^2 + FP^2)$, where FPH and FP are the derivative and native structure factor amplitudes, respectively. $R_C = \Sigma||FPH \pm FP| - |FH(cal)||/\Sigma|FPH \pm FP|$ for centric reflections. FH(cal) is the calculated heavy atom structure factor. $R_K = \Sigma|FPH(obs) - FPH(cal)|/\Sigma FPH(obs)$. P_p, phasing power, = $\langle FH(cal)/E\rangle$ (ISO) or $\langle 2FH''(cal)/E\rangle$ (ANO), where FH''(cal) is the anomalous component of the calculated heavy atom structure factor and E is the residual lack of closure error.

was applicable. On the basis of similarities in the subunit molecular weights, kinetic parameters and their pH dependence, and the ability to be activated by pyruvamide and inactivated by mechanism-based inactivators (Zeng et al., 1993), PDCs from the two strains are expected to be highly homologous, and the *S. cerevisiae* sequence indeed fit the electron density map extremely well. Also, we recently obtained crystals from the *S. cerevisiae* strain which are isomorphous to the *S. uvarum* crystals and give X-ray data having a merging *R* factor of 0.08 with the earlier data, further substantiating the homology assumption. The initial model was then improved, extended, and refined against the 2.4-Å native data by several cycles of simulated annealing (program XPLOR; Brunger et al., 1987), manual rebuilding, and restrained least squares (program GPRLSA; Furey et al., 1982).[2] A final examination of omit maps at 2.4-Å resolution (deleting 10–20 residues at a time) provided only two clear-cut indications of deviation from the *S. cerevisiae* sequence: R55 → A55 and V538 → I538. Accordingly, we expect any additional sequence changes to be minor. Two short segments in the chain are badly disordered (in addition to the N-terminal Met and seven residues at the carboxy terminus) and were omitted from the model. The final model contains two independent monomers, each with 537 amino acids out of a possible 563, and two ThDP, Mg cofactor pairs. This model includes restrained individual thermal factors, but no solvent other than the two waters coordinated to the Mg^{2+} cofactors. The *R* factor is 0.197 for all data between 10- and 2.4-Å resolution with $I > 2\sigma(I)$. The rms deviations from ideality for bond distances and angles are 0.015 Å and 3.4°, respectively. Only 6 of the 1074 residues have ϕ/ψ values in unfavorable regions of the Ramachandran plot.

RESULTS

(*A*) *Domain Structure and Folding Pattern.* Each PDC monomer contains a single polypeptide chain which folds into three roughly equal sized structural domains, denoted as α, β, and γ according to their consecutive locations along the N- to C-terminal direction. The domain centers lie on vertices of an approximately equilateral triangle with lengths of roughly 32 Å. All three domains have a mixed α/β topology as shown in Figure 2. The α and γ domains have essentially the same fold, although they share little sequence homology. The folding motif there is similar to that in NAD binding domains which also have a central six-strand parallel β sheet flanked by α helices; however, the sheet connectivity differs. The α- and γ-domain folding pattern was recently reported for one of the domains in the ThDP-dependent enzyme transketolase (Lindquist et al., 1992); thus it is likely to be characteristic of ThDP-dependent enzymes in general, although it was also found in one other non-ThDP binding protein (Shaw & Muirhead, 1977). There is no interpretable electron density for residues 106–113 in the α domain, which constitute an exposed loop.

The β domain contains a seven-strand mixed sheet, with five strands parallel and the others (located at one end) antiparallel. As in the α and γ domains, in the parallel part all crossover connections are right-handed and involve helices. There is no interpretable electron density for residues 292–301, which serve as a crossover connection between two parallel strands.

(*B*) *Dimer and Tetramer Association.* Two monomers in a crystallographic asymmetric unit are tightly associated to form a dimer with approximate 2-fold symmetry (rms deviation of 0.98 Å for Cα atoms). Within the dimer, monomer–monomer contacts are exclusively between residues in the α and γ domains. A 2-fold rotation of the dimer about the *b* axis generates another dimer, which contacts the first to form a complete PDC tetramer with approximate 222 point symmetry as deduced earlier (Dyda et al., 1990, 1991). Dimer–dimer contacts within the tetramer are almost exclusively confined to the β domains. These contacts are mainly between the last antiparallel strand in each domain, such that the two mixed sheets merge to form a large, continuous 14-strand twisted sheet. Contacts between monomers within each

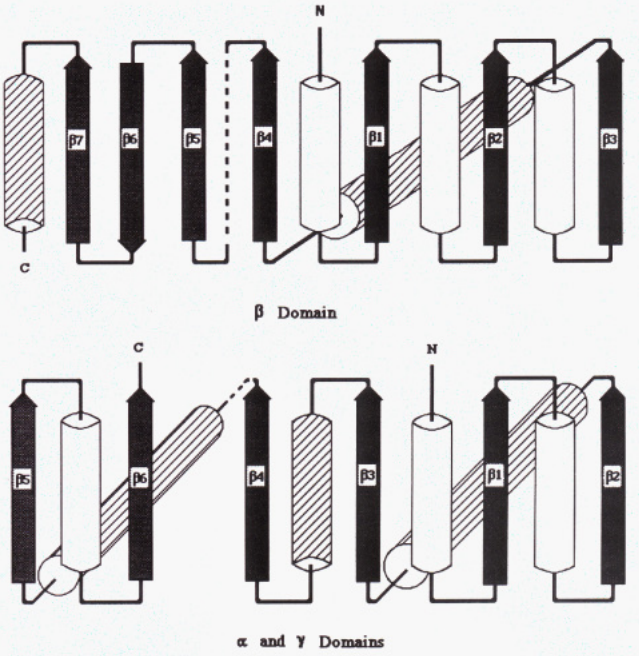

FIGURE 2: Topology diagrams showing the chain fold for the α, β, and γ domains. Cylinders represent one or more α helices; arrows represent β strands. Shaded cylinders are behind the β sheet; open ones, in front. Dotted lines indicate disordered regions in the α and β domains where the model could not be fit. There is no disorder in the γ domain.

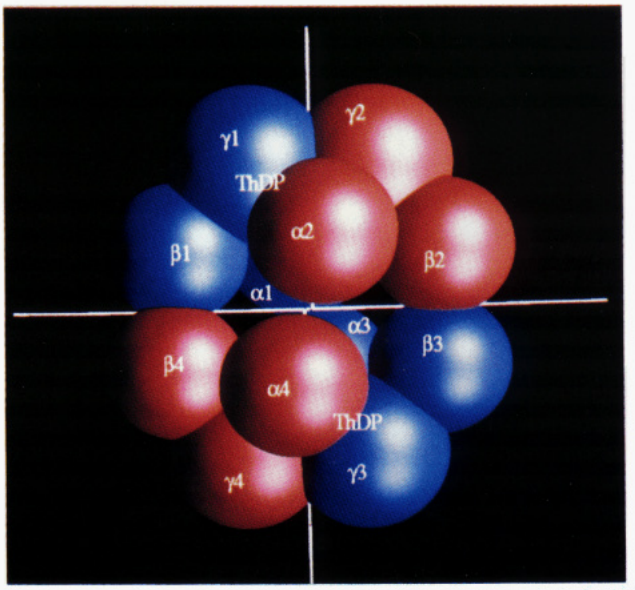

FIGURE 3: Schematic diagram indicating the domain and monomer association within the tetramer, viewed roughly down the crystallographic *b* axis. The 2-fold and pseudo-2-fold axes are indicated, as are the approximate locations of the catalytic sites. There are additional catalytic sites (not shown) at the α1–γ2 and α3–γ4 interfaces on the back side of the tetramer. Monomers of the same color are related by exact (crystallographic) 2-fold symmetry.

[2] GPRLSA is a local version of PROLSQ; Hendrickson & Konnert, 1980.

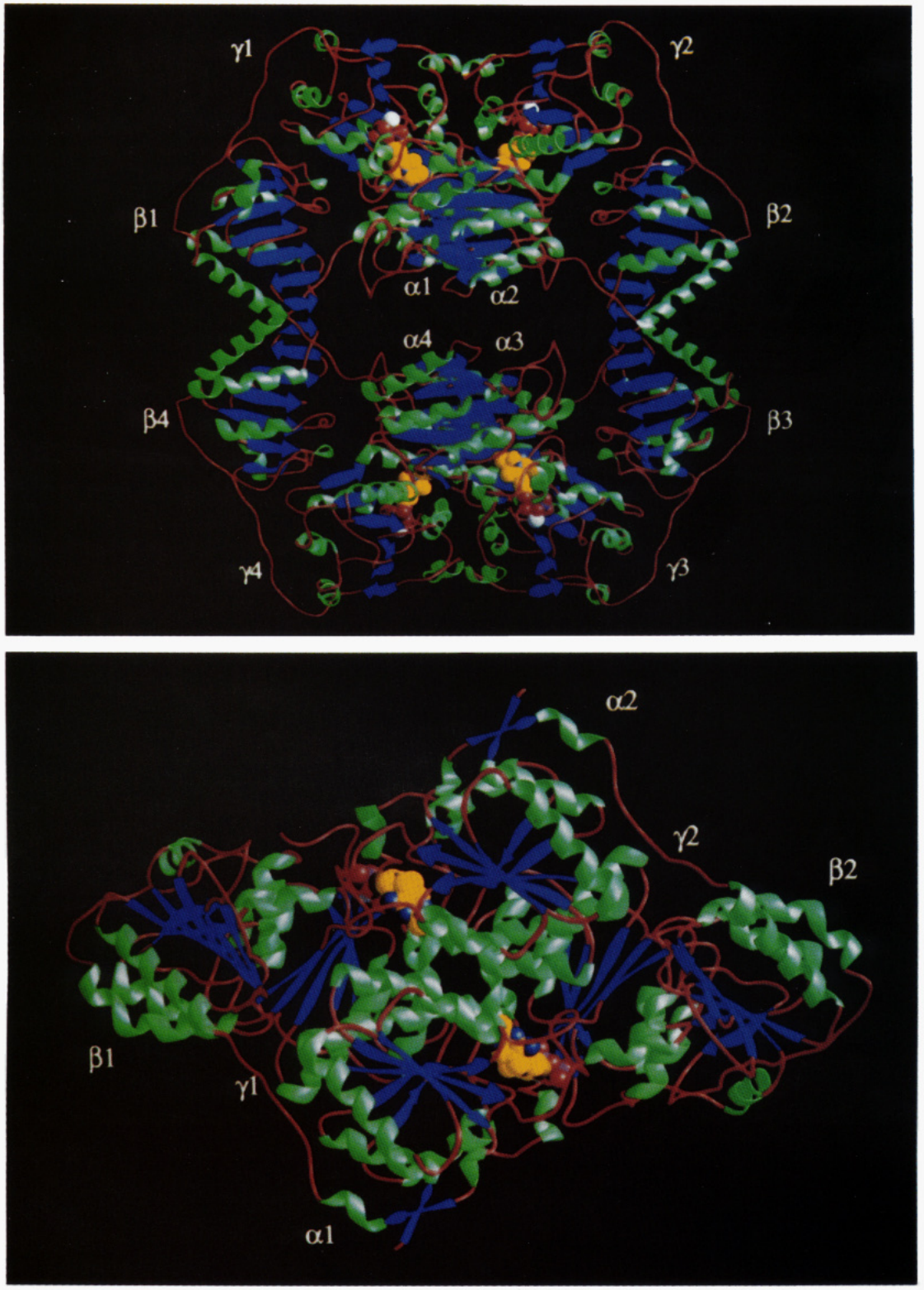

FIGURE 4: Ribbon drawings (Carson & Bugg, 1986) of the complete tetramer (a, top) and dimer (b, bottom). The tetramer is viewed roughly down the crystallographic *b* axis as in Figure 3; the dimer is viewed down the local 2-fold axis (vertical axis in Figure 3). The cofactors are included with a space-filling representation.

dimer are both tight and extensive, traversing the entire length of the molecule. On the other hand, contacts between dimers in the tetramer are few in number and are limited to small regions only at the end of the mixed sheets. Accordingly, the PDC tetramer is loosely associated and is best described as a dimer of dimers. Evidence for such an association in solution was also recently reported (Konig et al., 1992). A schematic diagram showing the domain and monomer association within the tetramer is given in Figure 3. Ribbon drawings of the tetramer and dimer are given in Figure 4.

(*C*) *Cofactor Binding and Active Site Structure.* The ThDPs are situated at the interface between monomers within each tightly associated dimer, with two sites per dimer and four per tetramer. The diphosphate end of the cofactor is associated mainly with the γ domain of one monomer, while the aminopyrimidine end is primarily associated with the α domain of the other monomer. In both the α and γ domains, the ThDP binding site is located in a crevice formed at the carboxyl end of the β sheet, precisely at the "topological switch point" (Branden, 1991). Anchoring of ThDP is achieved via

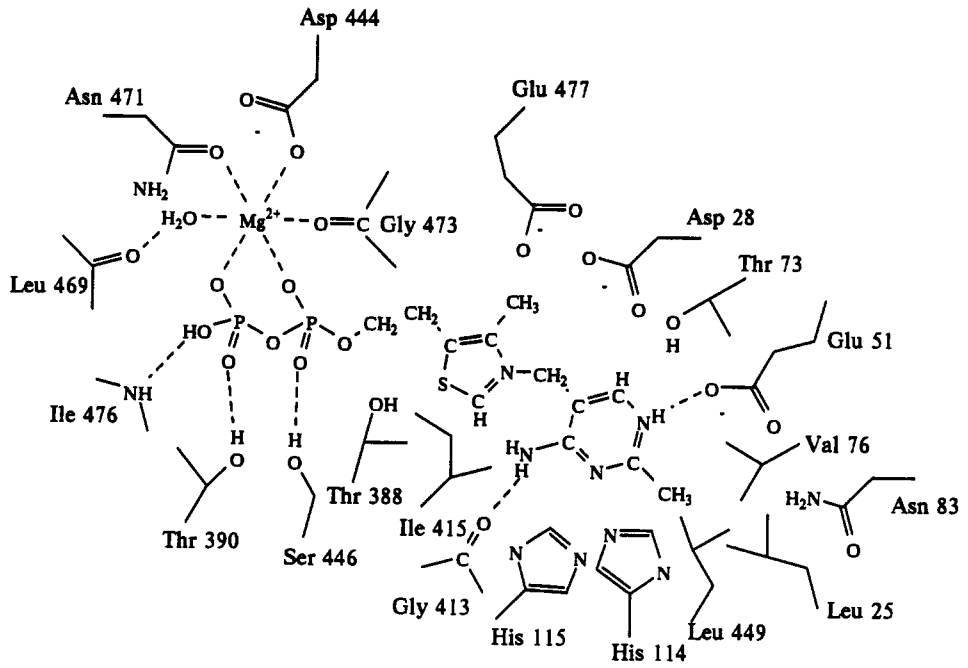

FIGURE 5: Schematic diagram of the dimer interface environment around the catalytic center. Bonding interactions between cofactors and protein are indicated by dashed lines. Residues numbered >360 are in the γ domain of one monomer, while those <187 are in the α domain of the "other" monomer.

the diphosphate which forms a complex with Mg(II), as well as through hydrogen bonds to the protein. The Mg(II) is coordinated with octahedral geometry and is bound to side-chain oxygens of D444 and N471, to the carbonyl oxygen of G473, to two diphosphate oxygens, and to a water molecule also bound to the carbonyl oxygen of L469. The diphosphate oxygens further hydrogen bond to the side chains of S446 and T390 and to the main-chain nitrogen of I476. The aminopyrimidine end forms hydrogen bonds between N1′ and the side chain of E51 and between N4′ and the carbonyl oxygen of G413.

The ThDP cofactor is buried in a cavity approximately 10 Å wide and 8 Å deep and is found in the "V" conformation (Shin et al., 1977) with the torsion angles (Sax et al., 1974) $\phi_t = 95.5°$ and $\phi_p = -65.9°$. Apart from the hydrogen bonds to the aminopyrimidine ring, the V conformation is stabilized (and imposed by the protein matrix) by strong van der Waals interactions with the side chain of I415, which is wedged tightly between the two aromatic rings. The conformation thus forces the 4′-amino group to be within interaction distance of the C2 reaction center. The walls of the cavity leading to the reaction center are lined with the hydrophobic residues I480, I476, F393, V410, and T388 toward the thiazolium ring side and with the hydrophilic residues H114, H115, and D28 toward the aminopyrimidine ring side. The active center is deeply buried, such that only the S, C2, and N4′ atoms are accessible from the solvent. Residues in the vicinity of the active center and close enough to potentially interact with reaction intermediates include D28, E477, T388, H114, and H115. The cofactor environment is shown in Figure 5.

DISCUSSION

The roles of D444 and N471 in binding cofactor to enzyme, observed in both PDC and their counterparts in transketolase, now firmly establish the importance of a conserved sequence roughly 30 residues long (Hawkins et al., 1989) starting with GDG and terminating with NN. These residues are among the few highly conserved in all ThDP-dependent enzymes and form the Mg(II) binding site which assists in anchoring the diphosphate to the protein matrix.

Interestingly, no potential general base, except for the 4′-amino nitrogen, is poised to ionize the C2H to initiate the reaction. How is this amino group activated? The presence of a conserved hydrogen bond to N1′ (from E51) suggests that the model developed some years ago (Jordan & Mariam, 1978; Jordan et al., 1982) may be operative: if E51 maintains the N1′ atom in the protonated state, that induced positive charge would help to ionize the 4′-amino group by lowering its pKa, converting it to an imino tautomer capable of accepting a proton. The presence of a hydrogen bond from N4′ to G413, on the side opposite to the thiazolium C2, supports such a hypothesis. As of now, we do not favor involvement of a histidine in the aminopyrimidine activation (as suggested for transketolase; Lindquist et al., 1992), since H115, while only ca. 4 Å from N4′, orients its nitrogens to hydrogen bond with D28 and the carbonyl of W412 so that these potential hydrogen-bonding atoms do not make short contacts with N4′.

It had been reported by several groups that reconstitution of apo-PDC (devoid of its cofactors) with ThDP quenches the intrinsic PDC fluorescence (Biaglow et al., 1969; Farzami et al., 1977; Jordan et al., 1988), suggesting interaction of coenzyme with a nearby tryptophan. In a recent study it was shown that the W493L mutant of PDC from *Zymomonas mobilis* is active (Diefenbach et al., 1992), but addition of ThDP leads to diminished fluorescence quenching compared to wild-type PDC. This points to W493 as the likely source of the fluorescence quenching. Surprisingly, W493 is far from the reaction center [11.6 Å from the Mg(II)], but it lies in the dimer interface, very close to the local 2-fold axis, and participates in ring stacking with F502 of the "other" monomer. Given that the ThDP cofactor is also deeply wedged in the dimer interface, a "burrowing" ThDP in the presence of binding to apo-enzyme could shift both domains slightly to disrupt interactions elsewhere across the interface, altering the ring stacking and thus the extent of fluorescence quenching.

Finally, it has long been reported that cysteine-specific reagents inactivate PDC, but surprisingly no Cys's are found closer than 20 Å from ThDP. Mechanism-based inactivation (unpublished) has been shown to label C221, and a fusion PDC possessing C221 as the only Cys is still activatable by

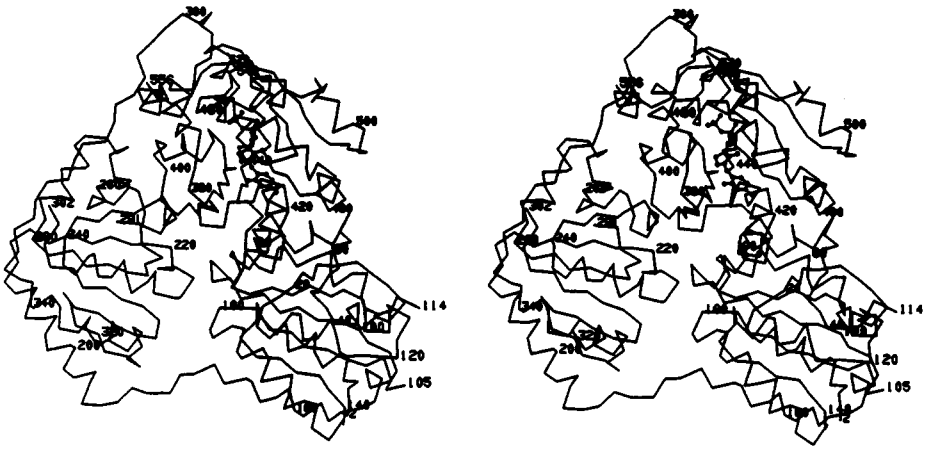

FIGURE 6: Stereoscopic α-carbon representation of an intact PDC monomer showing the relative positions of the α, β, and γ domains and catalytic and putative regulatory sites. The catalytic center is indicated by the "all-atom" representation for ThDP (only the cofactor associated with the γ domain of this monomer is shown). The putative regulatory agent binding site cavity is at the center where all three domains coalesce. The side chain of Cys 221 lines this cavity and is solvent accessible.

pyruvamide but is inactivatable by some other reagents (Zeng et al., 1993). C221 (β domain) is 22.6 Å from the active center but is accessibly positioned in a large cavity formed at the interface among all three domains. This cavity also lies precisely at the unoccupied "topological switch point" in the β domain and thus very likely encompasses the substrate activation site. Accordingly, inactivation of PDC by sulfhydryl reagents probably results from interference with the substrate (and pyruvamide) induced activation, thereby locking PDC into an "unactivatable" form. Organization of the monomer structure and catalytic and putative regulatory binding sites is shown in Figure 6. Specific details of the catalytic and regulatory machineries should emerge from further analysis of the structure and from similar analysis of complexes with various substrates, activators, mechanism-based inhibitors, and mutants.

ACKNOWLEDGMENT

The authors are grateful to the Anheuser-Busch Brewing Co., Newark, NJ, for their continuing generosity in supplying the brewers' yeast.

REFERENCES

Biaglow, J. E., Mieyal, J. J., Suchy, J., & Sable, H. Z. (1969) *J. Biol. Chem. 244*, 4054–4062.

Blum, M., Metcalf, D., Harrison, S. C., & Wiley, D. C. (1987) *J. Appl. Crystallogr. 20*, 235–242.

Boiteux, A., & Hess, B. (1970) *FEBS Lett. 9*, 293–296.

Branden, C. (1991) in *Introduction to Protein Structure* (Branden, C., & Tooze, J., Eds.) pp 49–51, Garland Publishing Co., New York.

Breslow, R. (1958) *J. Am. Chem. Soc. 80*, 3719–3726.

Brünger, A., Karplus, M., & Petsko, G. A. (1987) *Science 235*, 458.

Carson, M., & Bugg, C. (1986) *J. Mol. Graphics 4*, 121–122.

Crosby, J., Stone, R., & Lienhard, G. E. (1970) *J. Am. Chem. Soc. 92*, 2891–2900.

Diefenbach, R. J., Candy, J. M., Mattick, J. S., & Duggleby, R. G. (1992) *FEBS Lett. 296*, 95–98.

Dyda, F., Furey, W., Swaminathan, S., Sax, M., Farrenkopf, B., & Jordan, F. (1990) *J. Biol. Chem. 265*, 17413–17415.

Dyda, F., Furey, W., Swaminathan, S., Sax, M., Farrenkopf, B., & Jordan, F. (1991) in *Biochemistry and Physiology of Thiamin Diphosphate Enzymes* (Bisswanger, H., & Ullrich, J., Eds.) pp 115–122, VCH Publishers, New York.

Farrenkopf, B., & Jordan, F. (1992) *Protein Expression Purif. 3*, 101–107.

Farzami, B., Mariam, Y. H., & Jordan, F. (1977) *Biochemistry 16*, 1105–1110.

Furey, W., & Swaminathan, S. (1990) in *American Crystallographic Association Meeting Abstracts*, PA33, New Orleans, LA.

Furey, W., Wang, B. C., & Sax, M. (1982) *J. Appl. Crystallogr. 15*, 160–166.

Gallo, A. A., & Sable, H. Z. (1982) in *Thiamin Twenty Years of Progress* (Sable, Z. H., & Gubler, C. J., Eds.) Vol. 378, pp 78–90, New York Academy of Sciences, New York.

Hawkins, C. F., Borges, A., & Perham, R. N. (1989) *FEBS Lett. 255*, 77–82.

Hendrickson, W. A., & Konnert, J. H. (1980) in *Biomolecular Structure, Function, Conformation and Evolution* (Srinivasan, R., Ed.) Vol. 1, pp 43–57, Pergamon, Oxford.

Hohmann, S. (1990) in *Biochemistry and Physiology of Thiamin Diphosphate Enzymes* (Bisswanger, H., & Ullrich, J., Eds.) pp 106–114, VCH Publishers, New York.

Howard, A. J., Gilliland, G. L., Finzel, B. C., Poulos, T. L., Ohlendorf, D. H., & Salemme, F. R. (1987) *J. Appl. Crystallogr. 20*, 383–387.

Jones, T. A. (1978) *J. Appl. Crystallogr. 11*, 268–272.

Jones, T. A., Zou, J. Y., Cowan, S. W., & Kjeldgaard, M. (1991) *Acta Crystallogr. A47*, 110–119.

Jordan, F. (1974) *J. Am. Chem. Soc. 96*, 3623–3620.

Jordan, F. (1976) *J. Am. Chem. Soc. 98*, 808–813.

Jordan, F., & Mariam, Y. H. (1978) *J. Am. Chem. Soc. 100*, 2534.

Jordan, F., Chen, G., Nishikawa, S., & Wu, B. S. (1982) in *Thiamin Twenty Years of Progress* (Sable, H. Z., & Gubler, C. J., Eds.) Vol. 378, pp 14–31, New York Academy of Sciences, New York.

Jordan, F., Akinyosoye, O., Dikdan, G., Kudzin, Z. H., & Kuo, D. J. (1988) in *Thiamin Pyrophosphate Biochemistry* (Schowen, R. L., & Schellenberger, A., Eds.) Vol. 1, pp 79–92, CRC Press, Boca Raton, FL.

Kluger, R. (1987) *Chem. Rev. 87*, 863–876.

König, S., Svergun, D., Koch, M. H. J., Hübner, G., & Schellenberger, A. (1992) *Biochemistry 31*, 8726–8731.

Lindquist, Y., Schneider, G., Elmer, U., & Sundström, M. (1992) *EMBO J. 11*, 2373–2379.

Sax, M., Pulsinelli, P., & Pletcher, J. (1974) *J. Am. Chem. Soc. 96*, 155–165.

Schellenberger, A. (1967) *Angew. Chem., Int. Ed. Engl. 6*, 1024.

Schellenberger, A., Hübner, G., & Sieber, M. (1988) in *Thiamin Pyrophosphate Biochemistry* (Schellenberger, A., & Schowen, R. L., Eds.) pp 113–121, CRC Press, Boca Raton, FL.

Shaw, P. J., & Muirhead, H. (1977) *J. Mol. Biol. 109*, 475–485.

Shin, W., Pletcher, J., Blank, G., & Sax, M. (1977) *J. Am. Chem. Soc. 99*, 1396–1403.

Weissman, L. (1982) in *Computational Crystallography* (Sayre, D., Ed.) pp 56–63, Clarendon Press, Oxford.

Zeng, X., Farrenkopf, B., Hohmann, S., & Jordan, F. (1993) *Biochemistry* (in press).